BERKELEY PUBLICATION
AND RESEARCH INTERNATIONAL
12.31.2020
Journal of Med., Biological and Pharm. Sci. Vol. 14 No. 3

DNA FORTIFIED POLYPYRROLE NANOWIRES FOR HEXANE AND AMMONIA SENSING

MANSUR YAHAYA IBRAHIM
Chemistry Department, Sokoto State University, Sokoto, Nigeria.

ABSTRACT

Polypyrrole DNA templated nanowires were created by using simple fabrication method that applied DNA as a template on which to carry out the polymerisation. Their morphology, chemical state and electrical properties were analysed by microscopic (AFM, TEM and SEM), spectroscopic (FTIR, UV-Vis and XPS) and current voltage measurement (I-V) methods respectively. The nanowire films with a diameter of 3-12 nm were tested for their ability to sense ammonia and hexane gases which resulted in good sensitivity of 98% to 0.61 ppm of NH_3 and 33% to 4.31 ppm of C_6H_{14} and ultrafast recovery of 45-85 s for ammonia and 28-92 s for hexane gas with high repeatability. The current transients demonstrate the reversible type sensing to the gases (NH_3 or C_6H_{14}) detection using as grown PPyDNA nanowire arrays sensor. Possessing good response recovery properties, linear dependence, repeatability, selectivity and long-term

Introduction:

Multicomponent supramolecular systems major advantages in sensing is that manipulation of the component can easily change its both recognition and read-out characteristics. Unique properties of conductive polymer nanocomposites derived from the successful combination of the qualities of parent constituents into a single material have made them to attract a lot of research interest. Conducting polymers are being applied in several electronic devices [1]. Polypyrrole (PPy) is becoming increasingly important for it technological importance

ISSN: 1211-4401

stability, demonstrate their potential to be use as ammonia and hexane gases sensors.

Keywords: *DNA, Fortified, Polypyrrole, Nanowires, Hexane and Ammonia Sensing.*

due to its considerable electrical, optical properties and high chemical and electrical stability at ambient conditions [2]. It is particularly, a good candidate for solar cells, electrochromic displays, sensors, and high power super capacitors among others, within unique property of non-metallic temperature dependence conductivity [3]. It is a relatively air-stable with good environmental stability [4]. In recent times it have gained popularity as competent sensing materials for various organic vapours, hazardous gases and humidity due to fast charge-discharge mechanism which is proportional to it structure, high conductivity cause by high charge density and physico-chemical properties which are not easily altered by an external impulse[5]. It can be stabilized by counter ions incorporation into the polymer matrix during synthesis process, because polarons and bipolarons are greatly considered as the charge carriers in it [6].

Recently increasing concern for human health and environmental concern have made the detection of ammonia (NH_3) and hexane (C_6H_{14}) at low levels (ppm or ppb) a high priority. Based on United State Occupational Safety and Health Administration (US-OSHA) 35 ppm for 15 minutes exposure and 8 hours exposure limit of 25 ppm by volume are the permissible limits for NH3. It has vast industrial applications, especially in fertilizer and fine chemicals production. Exposure to high concentrations of ammonia in air causes immediate burning of the eyes, nose, throat and respiratory tract and can result in blindness, lung damage or death. Inhalation of lower concentrations can cause coughing and nose/ throat irritation [7].

Hexane is a chemical commonly extracted from petroleum and crude oil. It is a colourless liquid that gives off a fine, gasoline-like odour. It is highly

flammable, yet it serves a number of industrial and domestic purposes and can be found in many household products such as stain removers for arts, as a special glue used in roofing, shoemaking and leather products among others. The National Institute for Occupational Safety and Health (NIOSH) has set time weight-average limit of 50 ppm (180 mg/m^3) for normal hexane and a recommended exposure limit (REL) for hexane isomers of 100 ppm (350 mg/m^3) over an 8-hour workday. Short-term exposure to air contaminated with hexane affects the nervous system and can cause dizziness, nausea, headaches, and even unconsciousness. Chronic exposure can cause more severe damage to the nervous system. If swallowed, it may cause severe abdominal pain and impact the respiratory system, resulting in shortness of breath, coughing, burning of the mouth, throat or chest, and even chemical pneumonitis [8].

Current gas sensors operate at high temperatures and are very expensive to produce. With emission regulations becoming more and stricter, accurate and reliable room temperature gas sensors are necessary to regulate ammonia and hexane emissions Without these sensors, compliance with emission regulations is difficult since it is unknown how much harmful emissions are being put into the atmosphere [9].

Experimental section

Chemical Preparation of Polypyrrole/DNA Nanowires

This involved the thoroughly mixing of freshly distilled (under N_2) Py (5 µL; 3mM), λ-DNA solution (20 µL; 500 ng µL^{-1}) and $MgCl_2$ (5 µL; 0.5 mM). $FeCl_3$ (5 µL; 1 mM), an oxidant, was added and the solution was mixed and incubated at room temperature.

Samples preparation for Spectroscopic, Microscopic and Electrical Measurements

5 µL of the prepared PPyDNA nanowires films were drop-cast on clean Si (100) substrate and left to dry for 1h prior to measurements. For electrical measurements 2 µL drop of an aqueous solution of nanowires was placed on Pt microband electrodes and aligned across the gap between the Au fingers by molecular combing.

Measurement of Gas-sensing characteristics

Polypyrrole/DNA templated nanowires gas sensing test experiments were carried out by depositing 5 µL of nanowires solution between Platinum electrodes the gas sensing potentials of PPyDNA nanowires were investigated by recording their electrical responses when exposed to different gas mixture.

Results and Discussion

FTIR Studies

The FTIR spectrum obtained for PPy in aqueous media (Fig 1) shows the presence of characteristic transmission peak at 1529 cm^{-1} (C = C stretching of pyrrole ring), the single peak located at 1466 cm is assigned to a combination of C=C stretch, C-N stretch, and the deformation of the five membered ring which contains the C=C-N, C=C-C deformation [10], 1139 cm^{-1} (C-H in plane deformation), 1011 cm^{-1} (N-H in-plane deformation), 722 cm^{-1} (C-H out-of-plane ring deformation) and 653 cm^{-1} (C-C out-of-plane ring deformation or C-H rocking) [12]. All the above observed transmittance characteristics confirm the formation of PPy.

Previous work [12] has shown that templating PPy on DNA depends on the non-covalent interaction of the nascent polymer chains with the template. For instance, the symmetric PO_2^- vibration at 1097 cm^{-1}, the P-O/C-O stretches of the phosphate backbone at 1071 cm^{-1} and the asymmetric PO_2^- vibration at 1246 cm^{-1} are all shown to be reduced in the intensity and shifted by 16, 6 and 34 cm^{-1} to lower frequency, respectively in Watson et al. ,work [13].

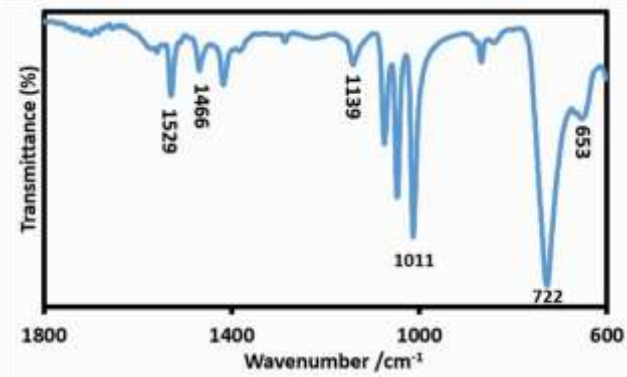

Figure 1: Transmission FTIR spectra of PPy. 128 scans co-added and averaged, 4 cm^{-1} resolutions

Figure 2 is a joined transmission spectra plot of PPyDNA and DNA, that shows in-plane vibration of cytosine and Guanine peaks in both PPyDNA (1519 cm^{-1}) and DNA (1535 cm^{-1}), that is a lower peak shift of 16 cm^{-1} in the PPyDNA, similarly the transmission bands of the two compounds at 1659 cm--1

(PPyDNA), and 1690 cm (DNA), which are assigned to the Thymine (C2 = O stretching) [14].

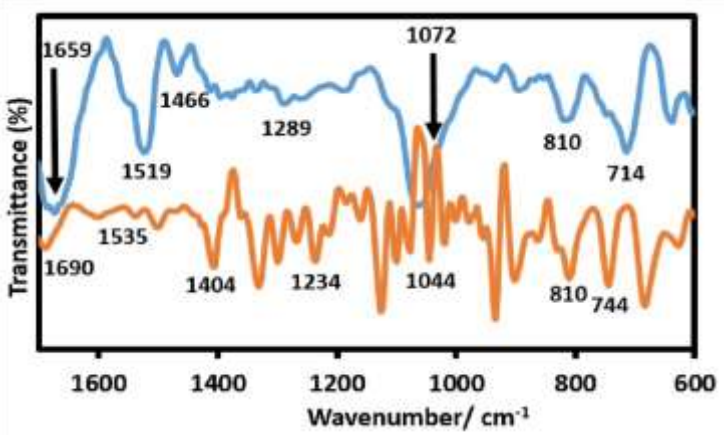

Figure 2: Transmission FTIR spectra of PPyDNA (blue) and DNA (orange).

In Table 1 various shifts in the peak position change can be seen in PPyDNA spectrum when compared to the corresponding bands in the spectrum of free DNA. For instance, the ring deformation out-of-plane-bending (PPyDNA, 714 cm^{-1}) peak, shifted to lower frequency when compared to the DNA(744 cm-1) spectra, on the other hand C-O deoxyribose stretch/ PO_2^- symmetric stretching; asymmetric PO_2^- stretch and in-plane vibration of cytosine (1044, 1234 and 1404 cm^{-1} in DNA) were found to shift to high frequency in the PPyDNA nanowire (1072, 1289 and 1466 cm^{-1}).

Furthermore, both substances have same spectral values at 810 cm^{-1} which correspond to Deoxyribose, B-marker. Generally bands observed in the 800-1800 cm^{-1} region of the spectrum further confirm the presence of DNA in the hybrid material. These features can be assigned to nucleobase

vibrations as well as stretches associated with the phosphate backbone [15].

Table 1: Selected bands in DNA and PPyDNA spectra and their assignments

Wave number in DNA (cm^{-1})	Wave number in PPyDNA (cm^{-1})	Peak Shift (cm^{-1})	Assignment
744	714	-30	Ring deformation out-ofplane-bending
810	810	0	Deoxyribose, B-marker
1044	1072	+28	C-O deoxyribose stretch/ PO_2^- symmetric stretching
1234	1289	+55	Asymmetric PO_2^- stretch
1404	1466	+62	In-plane vibration of cytosine

The FTIR spectra indicated that the PPyDNA sample is not a simple mixture of DNA and PPy but rather an intimate interaction of DNA with PPy in the hybrid polymer because of the several notable shifts in their peak positions and intensities observed.

UV-vis Studies

The extent of mixing of PPy and DNA in PPyDNA was evaluated in this work by UV-vis absorption spectroscopy and displayed in figure 3.In both the spectra of PPy and PPyDNA, the absorption band in the range of 210 to 246 nm corresponds to the $\pi^*-\pi$ transition resulting from the formation of polypyrrole. A broad absorption band starting from 310 to 366 nm (indicated by a square, in spectrum of PPy) corresponds to a bipolaron transition, a characteristic feature for the oxidized state of polypyrrole [22]. The 260 nm band observed in the spectra of free DNA have shifted to

210 nm in the PPyDNA spectrum which is an indication of the mixing of PPy and DNA.

Sree et al. [17] suggested in their work that the changed π-bond chromophore of indene/pyrrole aromatic ring system in ClnPy nanomaterial is due to overlapping of phenyl π -conjugated unit and skeleton of pyrrole monomer and is possibly responsible for the blue shifted and broadened absorption peak. These additional absorptions suggest π-π* electron transitions in the band gap of the conjugated pyrrole ring system, existing in CInPy polymeric chain which is similar to our work.

The continuous variation of wavelength and intensity of UV-Vis bands may result from the copolymerization effect of PPy with DNA. That is to say, the polymer formed by oxidative polymerization of PPy with DNA is a complex mixture of two substances rather than the mixture of two homopolymers

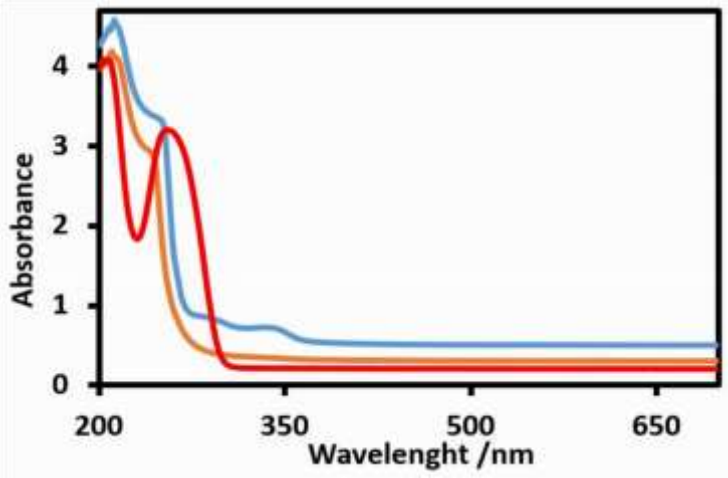

Figure 3: UV- Vis absorption spectra at different stages of the synthesis process: absorption spectra of aqueous PPy solution (blue); free DNA (red) and PPyDNA (orange).

XPS studies

To determine the elements and chemical-bonding state of the compounds in the PPyDNA, nanowires, the X-ray photoelectron spectroscopy (XPS) analysis of the samples was studied with the binding energy obtained in the analysis calibrated using carbon (284.8 eV) as a reference. XPS survey spectra of PPyDNA samples (Figure 4) exhibit the presence of the elements

C, N, O, Cl (which originated from the oxidant used or from $MgCl_2$ that was used in the preparation), and (weakly) P. Clear evidence for the presence of DNA in the sample material was obtained from the P2p signal at 133.2 eV, arising from the phosphorus in the phosphodiester backbone of the DNA. No signature of the presence of iron was observed in the survey spectra which confirm that the $FeCl_3$ was used only to drive the polymerisation without any oxidative damage to DNA.

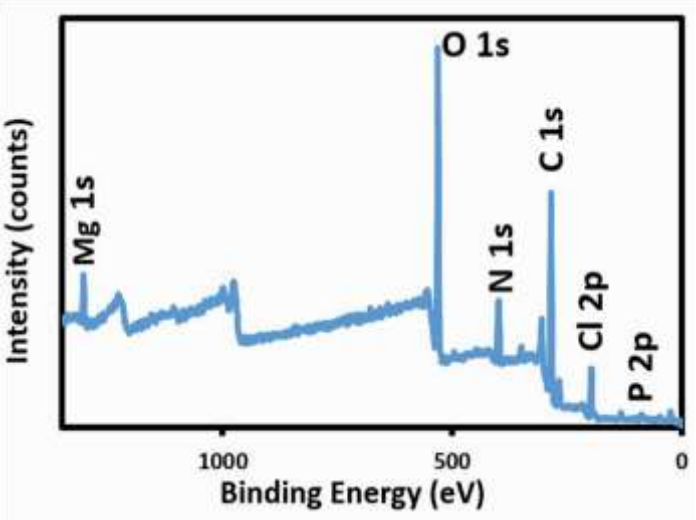

Figure 4: XPS Survey scan chart of PPyDNA nanowire at pass energy of 20 eV and the step size of 0.3 eV.

The Cl_2p peak in the survey spectrum reveals the presence of the Cl in the sample; this suggests that the anionic charge of the DNA is not sufficient to compensate the cationic charge of the bound PPyDNA, and that Cl^- anions are also present as dopants in the material. Finally, the survey scan shows the absence of Fe in the sample which indicates that it is not incorporated in the material to any significant extent. Consequently, these XPS spectra confirm that PPyDNA nanowires incorporating $FeCl_3$doping agents are obtained from the oxidation of pyrrole in aqueous solvents.

Figure 5a and b revealed the C1s and N1s spectra of PPyDNA nanowire. The C1s signal can be fitted by three different carbon species at 284.8, 286.6 and 288.3 eV. The first component at the lowest binding energy (284.8 eV) relevant to β and α carbon atoms, revealed the first fascinating finding.

Actually, the comparison of this carbon atom areas showed that, due to over oxidation, the β carbons in the film were less abundant than the α ones. This indicates, that the β positions were the ones involved in the polymer functionalization. The second peak at 286.6 eV is attributed to carbons of the polymer C=N or C - N^+; the third one at 288.3 eV to C= N^+ carbons and the peak much weaker at 284.8 eV to carbonyl C=O groups. The appearance of a C=O component may be associated with the over oxidation of PPyDNA at the β carbon site in the pyrrole rings [18].

The C (1s) component occurring between 286.1 and 286.4 eV can arise from a number of different sources. Some researchers attribute this band in polypyrrole to disorder type carbons, which they define as being cross linked, chain-terminating and non -α, α' bonded carbons as well as partially saturated rings. There will also be a small contribution from unavoidable hydrocarbon contaminants, while othershave suggested that electrostatic interaction of ring in carbons with counter ions will also have an effect. The C (1s) component between 288 and 289 eV is generally attributed to carbonyl or carboxyl species resulting from chain termination. [19].

The PPyDNA nanowires show the expected principal C (1s) component at 284.8 eV arising from the pyrrole ring α and β carbons and methylene groups within the pendant side chain [20].

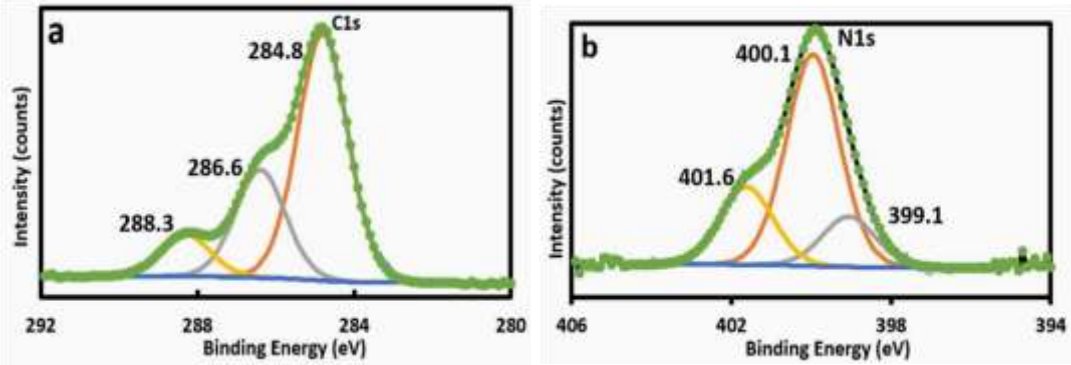

Figure 5: a) N is XPS Spectrum and b) C is XPS Spectrum of PPyDNA nanowires

The N1s spectra (Fig. 5b) indicate the presence of three peaks in the case of PPyDNA. It contains a two signals at 399.9 and 399.1 eV which are characteristic of pyrrolylium nitrogens (NH-structure) and a high Binding

Energy (BE) tail (BE = 401.6 eV) attributable to the positively charged nitrogen NH^+ (bipolaron).

The N (1s) region's two peaks located at approximately 400.1 and 401.6 eV, with the major component being the lower binding energy signal. This is in general agreement with other XPS studies of different polypyrrole species a number of which also show a small shoulder at ≈397 eV [21].

The main peak at 400.1 eV arises from the neutral pyrrole ring nitrogen, while the higher binding energy component is generally attributed to partially charged nitrogens within bipolaron sub-units. The presence of the shoulder at 399.1 eV depends, to some extent, on the experimental signal-tonoise ratio but also on the nanowires preparation conditions since it is more pronounced for neutral than as-prepared or oxidized polypyrrole [22].

Examination of the N1s peak provided evidence of the presence of DNA and polypyrrole in the sample material. Curve fitting of high resolution XPS spectra of the N1s region revealed two distinct peaks in the N1s envelope with binding energies at 399.5 and 401.4 eV (Figure 5b). Contributions to both of these peaks can be assigned to the presence of the DNA and polypyrrole.

Previous XPS studies of both free DNA [23] and polypyrrole [24] have reported that spectra of the N1s core level of these materials can be fitted to at least two separate components. The N1s core level of DNA, for example, has been reported to comprise of a lower binding energy peak (398.6– 399.0 eV) arising from the contributions of sp2- bonded N atoms in the nucleobase base rings and a higher binding energy peak (400.1-401.4 eV) attributed to the sp^3- bonded N atoms in the nucleobase rings and $-NH_2$ groups [25].

Similarly, polypyrrole is also known to give at least two distinguishable peaks of the N1s core level. In this study, a lower binding energy peak (399.1eV) tends to dominate, arising from the N-H groups present in the constituent pyrrolyl rings of the polymer. The higher binding energy species (400.1– 401.6 eV) arise from the presence of inequivalent nitrogen atoms in the polypyrrole structure, which occur as a result of their

electrostatic interaction with the dopant anions present in the polymer structure [26].

AFM Studies

Figure 6 shows the tapping mode AFM height images of water diluted bare DNA on Si/SiO_2 surface.

The images revealed network of DNA bundles with some rope like structures.

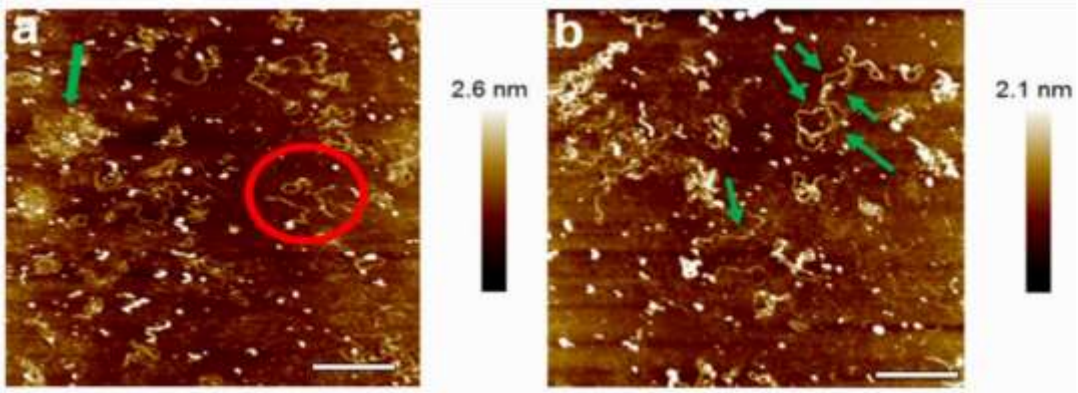

Figure 6: AFM height images of bare DNA on Si/SiO_2 substrate: (a) network of threadlike DNA bundles with some rope like structures being formed (b) zoomed image of the rope like molecule.

Threadlike DNA molecules are seen well spread out on the surface. The heights of the fibres in the network structures were estimated using height measurements of the DNA molecules obtained using the bearing function of the image analysis software (Bruker: NanoScope Analysis version 1.5) to calculate the height of the strands in 3 different spheres and it was found to be approximately 1.60 ± 0.01 nm, which is very close to dsDNA chain height, that was found to be about 1.5–2.0 nm reported in other study [27]. Proposed mechanisms for network formation from cyclic DNA include overlapping of DNA circles where divalent charged positive ions are serving as salt bridges not only between DNA and the surface, but also between it chains. Another similar mechanism for network formation by overcrossing of linear DNA chains was proposed to involve double strand splitting and triple strand DNA organisation. On the other hand, junction formation has been observed in short DNA networks of short DNA strands [28].

Figure 7 reveals the PPyDNA nanowires AFM height images, that shows different morphologies with materials indicating both small number of bare DNA strands, (a) proving that not all of the DNA in the reaction is involved in templating, well aligned polymeric nanomaterials with regular coverage extended across the substrate and high density PPyDNA films. In image (b) the height image shows a smooth morphology, consisting linear arrangement of nanomaterials densely packed. Mg^{2+} ions from MgCl2 were used to facilitate the adhesion of PPyDNA onto SiO2 substrate for best viewing and their presence may be responsible for the small white spots seen on the PPyDNA images.

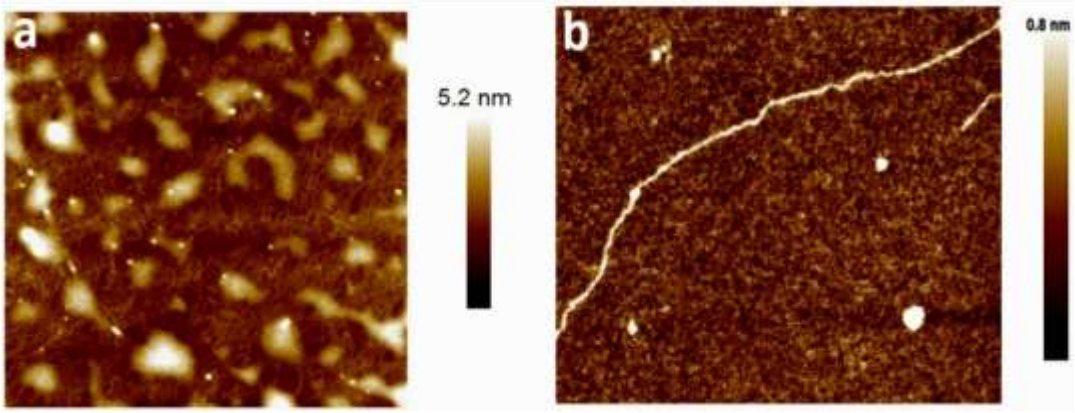

Figure 7: AFM height images: (a) nanowires films image showing the polymer materials incorporating/ bounding to the DNA material and aggregates of PPyDNA or non-templated polymer (b) well aligned, polymeric nanomaterials with regular coverage extended across the substrate.

Pruneanu and co-workers, [29] found that over longer periods of incubation, a self-assembly process occurs in which PPyDNA nanowires form rope-like structures which they called nanoropes, by carefully analysing the AFM images they believed that the assembly process that form the rope-like structures consists of individual nanowires twisted around each other. They showed that silanization can be used to control the density of the nanoropes on Silicon oxide which allow for connecting them in a two terminal electrical device that can measure their electrical properties.

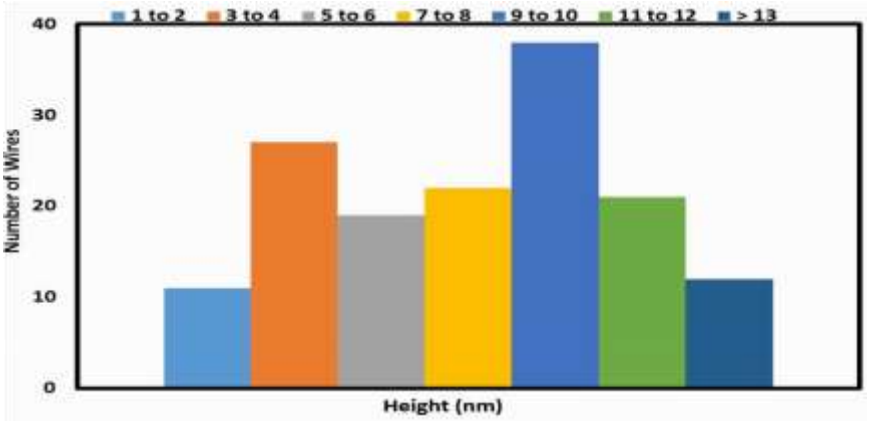

Figure 8: A histogram displaying the heights of 150 PPyDNA nanowires

From a more elaborate statistical analysis of the PPyDNA AFM height as shown in figure 8, the most common height, was 9-10 nm range, which can be attributed to previous research [30] explanations that on standing, the thickness of the nanowires appears to increase as the agglomeration process is gradual and continues for days, generating even thicker ropes. Small number of larger structures can be seen in the chart with diameters greater than 13 nm indicating the continuation of the polymerisation reaction after the nanowires formation.

TEM Studies

Transmission electron microscopy of the PPyDNA nanocomposite is shown in figure 9. The thick nanowires, is an indication of a large aspect ratio that also demonstrated that the polypyrrole nanomaterial coated the DNA strands to form an intimate nanocomposite into the DNA strands to form an intercalated nanocomposite. [31] Due to technical limitation of the TEM machine used, the size of the PPyDNA nanomaterials cannot be quantified.

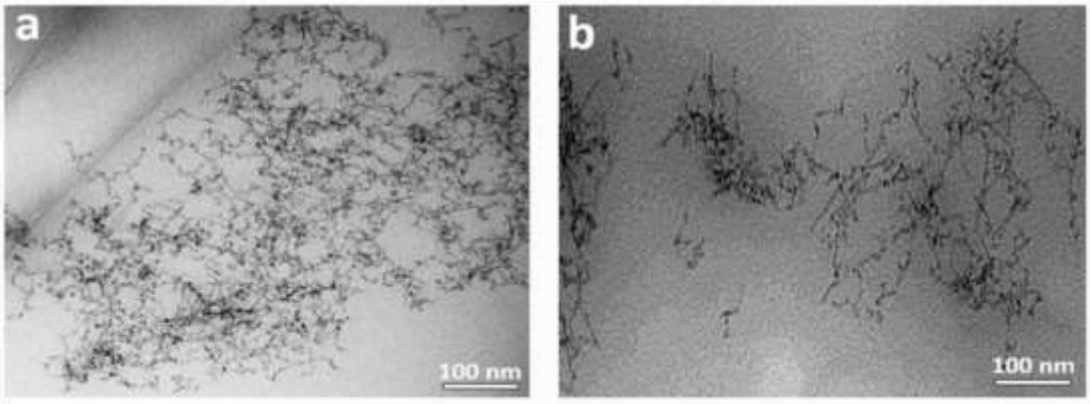

Figure 9: PPyDNA nanowires TEM images: (a) bee net like dense network structure of the nanomaterials films (b) magnified image from (a)

SEM Studies

Figure 10(a-d) displayed the SEM micrographs of undiluted and water diluted PPyDNA nanomaterials on treated silicon dioxide substrate, coated with gold, the materials shows a dense film of the undiluted DNA template polymers, On the order hand the water diluted nanomaterials revels a more loose or dispersed morphologies because of the dilution that may break their binding together.

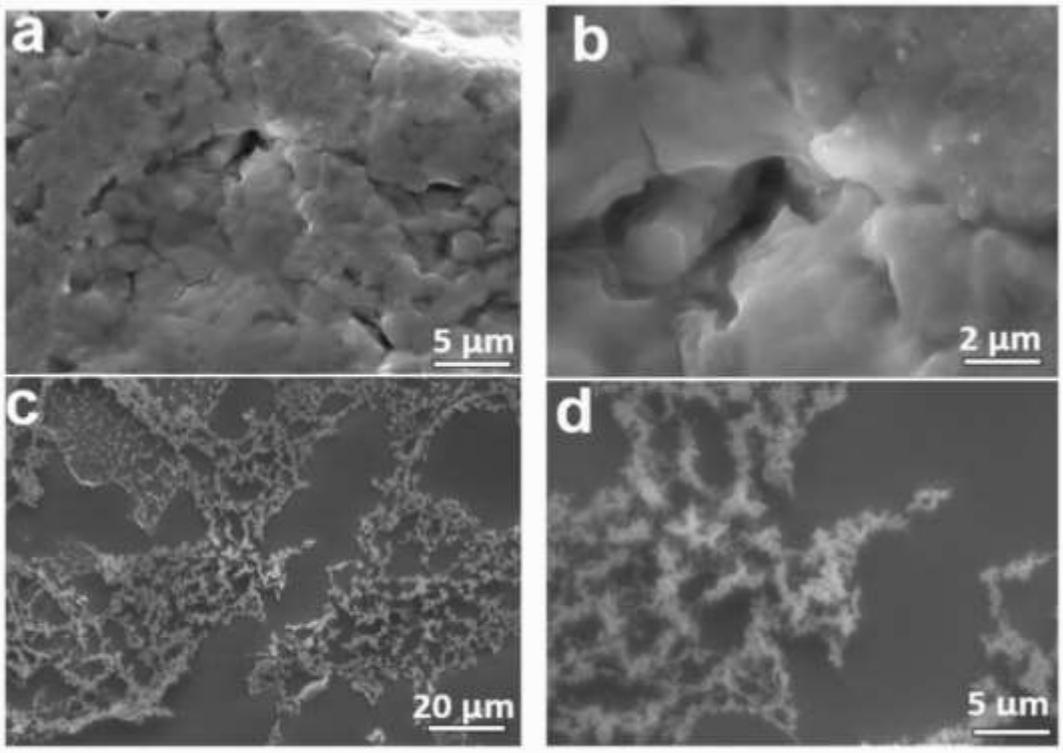

Figure 10: SEM micrographs of PPyDNA: (a) thick film of PPyDNA materials with carpet like morphology (b) zoomed image from (a) showing the thick film arrangement and (c) images revelling mesh-like morphology of individual wires after dilution with water (d) zoomed image of the nanomaterials from (b).

Many researchers have worked on SEM studies of polypyrrole composite. For instance, Su, et al. [32] polypyrrole SEM images, displayed a typically cauliflower-like or tumor-like structure. They suggested that the performance of three-dimensional (3D) pyrrole polymer growth can be considered as quasi network systems through the 2, 3 coupling mode.

Similarly polypyrrole powder showed a cauliflower-like morphology constituted by microspherical grains in Sanches et al. work. [33].

Generally, the SEM images from our studies imply the mixing of the polypyrrole with the DNA has a strong effect on the resulting templated nanomaterials' morphology. The composites show a transformation in morphology from typical free DNA thick films with the increase of polymer coating on the DNA and the interconnected morphology between the polypyrrole and DNA leads to a nanoscale surface roughness, which is likely to produce an enhanced mechanical interlocking and adhesion between the nanomaterial composites, which are suitable for gas sensing test as they can easily allow the flow of current when align on a micro electrode.

Two-Terminal Current – Voltage (I-V) studies

Current-Voltage sweepings, in the range of -5 to +5V at a constant temperature of 20^0C were measured. The bulk nanomaterials shows a significant current (micro amperes) when compared to Pt and DNA (10^{-14} A). The current-voltage control measurements support the assertion that the PPyDNA nanomaterials bridges are responsible for the electrical conduction, therefore they have electrical conductivity.

A significant contribution to resistance from electrical contact made between the PPyDNA nanowire and the Pt electrodes is possible, known as contact resistance which refers to the contribution to the total resistance of a material which comes from the electrical leads and connections as opposed to the intrinsic resistance of the wire, which is an inherent property, independent of the measurement method [34]. Contact is also traditionally applied for the consideration of the metal to semiconductor interface as a main contribution to this phenomenon. However, if the contact resistance is ignored, an estimate (lower bound) of the wire conductivity can be made.

The conductivity of any material changes with temperature and depending on the direction of this change it is possible to identify the nature of this material (metal, semiconductor and so on). The conductivity of an intrinsic

semiconductor increases with increasing temperature, because more valence electrons are exited into the conduction band, whereas it decreases in the case of metals (because of electron-phonon scattering) but in polymers the situation is different.

Current-voltage studies over a range of temperatures were performed in order to provide useful qualitative and quantitative information regarding I-V behaviour and to elucidate details of conduction mechanism. This method relies on the alignment of the nanowires by molecular combing across two micro fabricated Pt electrodes on a thermally oxidized Si chip. Variable-temperature I-V studies of the two-terminal device were performed over a temperature range of 223 to 423 K in order to elucidate details of the conduction mechanism.

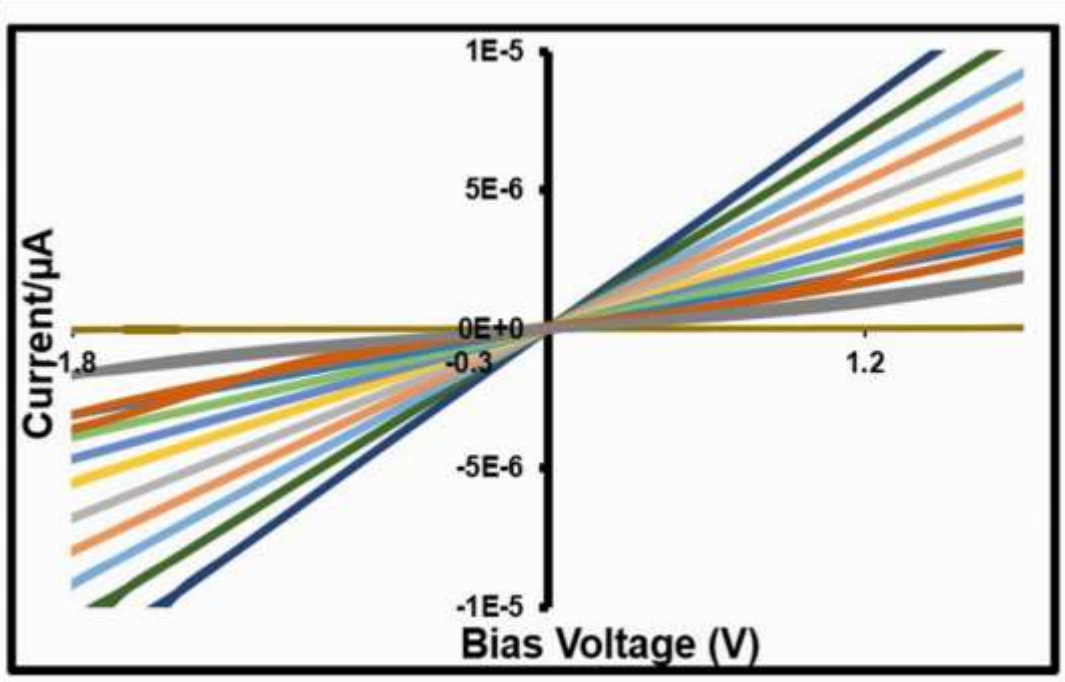

Figure 11: Current-voltage curves of a two-point contact PPyDNA nanowires at a temperature range from 223K to 423K

Current–voltage curves of PPyDNA nanowires device were recorded under nitrogen at sequence of temperatures in the range of 223 to 423 K. In Figure 11 the resulting I-V curves are presented. As can be seen the

current-voltage curves shows linearity at low bias voltages and exhibit a reproducible, linear response at a range of temperature. In addition, displayed increase in current output with increase temperature that is consistent with results of similar measurements of PPyDNA nanowires in other studies [35].

Conduction mechanism in polypyrrole can be explained in terms of the concept of polaron and bipolaron. Low level of oxidation of the polymer gives polaron and higher level of oxidation gives bipolaron. Both polarons and bipolarons are mobile and can move along the polymer chain by the rearrangement of double and single bonds in the conjugated system. The magnitude of the conductivity is dependent on the number of charge carriers available and their mobility. Temperature is proportional to the mobility of charge carriers, hence when they increase, a rise in conductivity will be observed. Another factor which affects the electrical conductivity is the molecular alignment of the chains within the entire system [36].

Analysis of the temperature dependence of conductance in conjugated polymers gives a more indepth of the conduction mechanism and is typically carried out through fitting conductance (G) values to the following equation:

$$= \quad - (\_\_) \qquad (1)$$

This expression is used when describing the conductance behaviour of a conjugated polymer system through a variable range hopping (VRH) model. This in turn describes the low temperature conductance behaviour in strongly disordered systems where electronic states are localized. In this approach, the outcome is dependent upon the dimensionality of the system which is described by the parameter $\beta=1/(1+D)$, where 'D' is the dimensionality of the system.

Figure 12 shows the corresponding Arrhenius plot of the conductance of the nanowires. The plot illustrates the temperature dependence of the rate constant and suggests simple electron hopping is the dominant mechanism for electron transport, shown through the exponential behaviour of the conductance upon increasing the temperature.

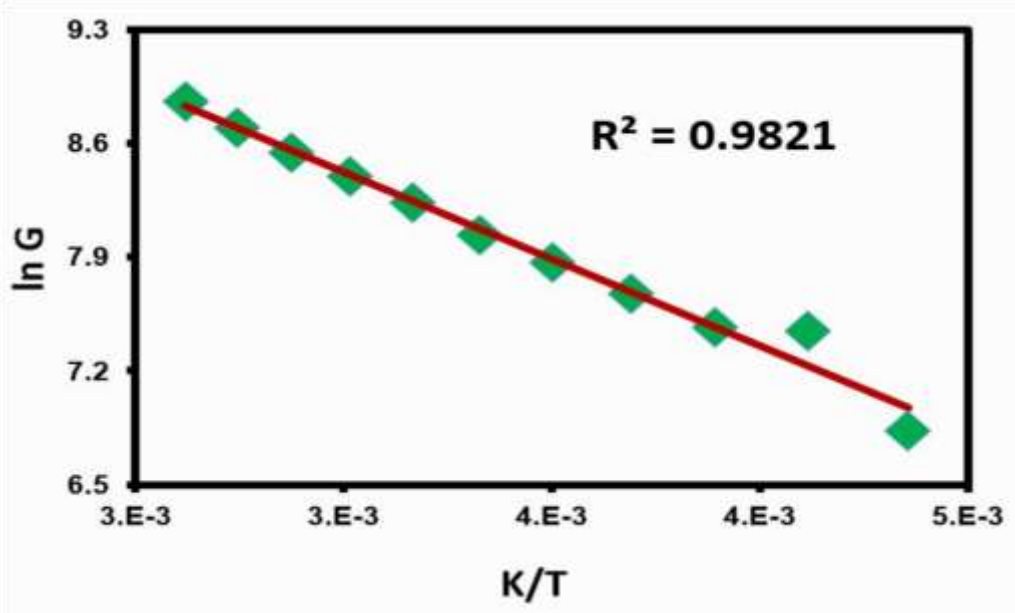

Figure 12: Arrhenius plot for the conductance G (S) of PPyDNA nanowires.

The slopes of the Arrhenius plots in figure 12 were analysed to determine the activation energies associated with the hopping of charge in these polymer nanowires sample. The bandgap of most conductive polymers is of order 3 eV that would predict Ea equal to 1.5 eV if the process were limited by thermal excitation across the gap. Instead, in our studies from table 2 Ea is <1 eV. This is because the process is thermally-assisted tunnelling between localized sites.

Ea values obtained from this study were compared with values from other bulk conductive polymers reported. Values from this research are greater than that of other studies, which may be due to conductivity of PPy that is proportional to the polymerisation temperature which is to hopping conductors; the charge carriers are considered to be substantially localized and make thermallyassisted tunnelling transitions or hops, between sites [37].

Sensing performance of the PPyDNA hybrid nanowires for ammonia and hexane gases detection

To compute the concentrations of gases analytes in our gas sensing test rig from the measured flow rates, mixing 100% of pure air flow rate and 100%

of saturated air passing through the Dreschel bottle equates to mixing equal amounts of pure air and of air saturated with the vapour so the resulting mixture will have a partial pressure half that of the saturated vapour pressure of the analyte material. Vapour pressure changes with temperature, so we record the laboratory temperature and look up the enthalpy of vapourization at that temperature and computed the vapour pressure at the actual laboratory temperature (temperature of the Dreschel bottle).

$$= \quad {}^{*}\frac{\qquad}{+} \qquad 2$$

Equation (2) was used to compute the partial pressure of vapour send to the sensor from the flow rates of air through the Dreschel bottle (Vv) and of pure V_{air} and * is the saturated vapour pressure of the analyte gas.

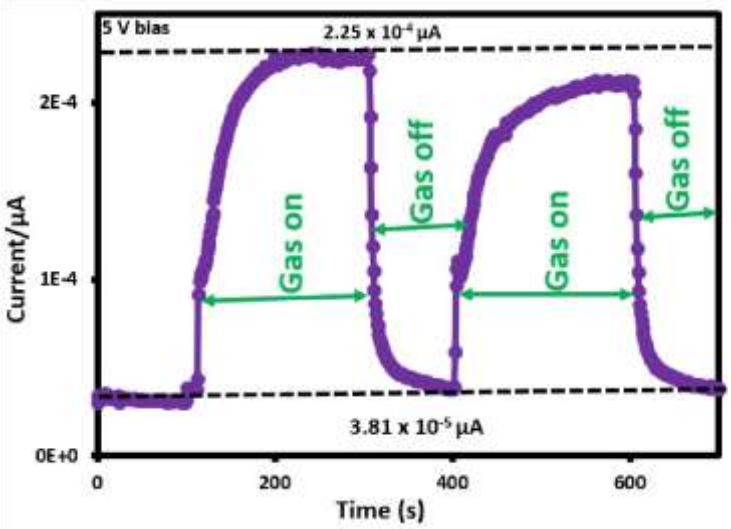

Figure 13: Schematic response graph of typical current transients of PPyDNA nanowires assemblage sensing films during detection of ammonia and hexane gases at room temperature and at a constant biased voltage of 5V.

Gas sensing processes can be classified into irreversible- when the base current/resistance recovers partially and reversible type, where the base current/resistance is fully recovered. The transient attribute of reversible

sensor during the response process are switched forth and back to the base in the presence and during the recovery process in the absence of the gas analyte respectively. These type of sensors are most commercially suitable because of their quick response and complete/full recoverable baseline [38].

Figure 13 illustrates the schematic response graph of typical current transients of PPyDNA nanowires assemblage sensing films during detection of ammonia and hexane gases at room temperature and at a constant biased voltage of 5V. The reproducibility in the response can be attributed to the adsorption and desorption of the analyte vapours during exposure and removal of vapours.

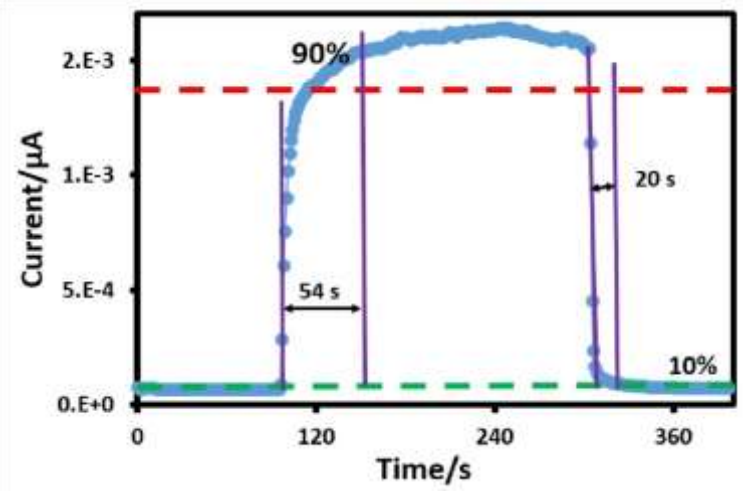

Figure 14: Schematic graph of response–recovery time for one cycle of PPyDNA nanowires sensing test

From figure 14 important parameters of gas sensors, the response and recovery times were derived. The response time (T_{90}) is defined as the time required for a sensor to reach 90% of the total response of the signal such as current/resistance upon exposure to the target gas in a sensor test chamber. Recovery time is defined as the time required for a sensor to return to 90% of the original baseline signal upon removal the target gas,

i.e the time to reach 10% conductance/resistance when analyte gas was turned off and air was reintroduced into the chamber.

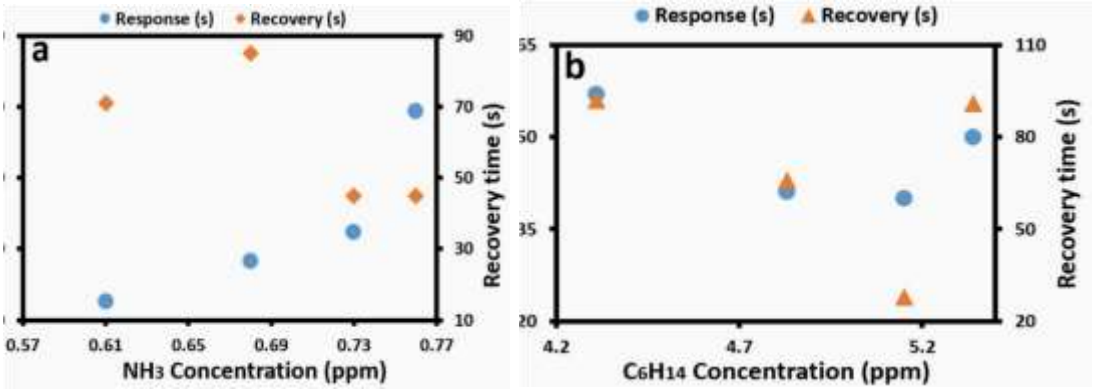

Figure 15: Variation of estimated response-recovery time with different NH_3 (a) and C_6H_{14} (b) concentrations during room temperature sensing with PPyDNA nanowires.

In NH_3 sensing the response time is in the range of 18 to 98 s to reach it current in the presence of different ppm concentration of its gas while in C_6H_{14} it is between 41 and 50 sas shown in figure 15(a-b). In NH_3 sensing, response time is faster than recovery time and it responded to PPyDNA nanowire faster (18 s) than C_6H_{14} (41 s) while the latter was recovered faster (28 s). It is observed that response time increases when the analyte gases concentration increases, which could be related to the number of occupied active site on the PPyDNA films increases as the gas molecules increases, with the augmentation of their concentration. For recovery time measurements C_6H_{14} was recovered faster (28 s) than NH_3 (45 s) for the different ppm concentrations of the gases. Both the response and recovery times are proportional to the concentration of the analytes.

The fast response and recovery times in both NH_3 and C_6H_{14} were constant for successive three sensing cycles for detection of different concentration of the analytes, which signifies that the chemically synthesised PPyDNA nanowires are stable for ammonia and hexane gases sensing representing good repeatability of flexible sensor. The PPyDNA nanowire sensors showed reversible and reproducible responses for each NH_3 and C_6H_{14}

vapour concentration, and their responses were more pronounced with increasing vapour concentration. These facts suggest that PPyDNA nanowires can be effectively utilized in detecting NH_3 and C_6H_{14} vapours of various concentrations.

The relative sensitivity ( ) of the gas sensor is defined as the ratio of the relative change in the conductivity (Δ) upon exposure to the gas being sensed with respect to its conductivity in an air ambient ( ):

Δ –

(%) = ___ × 100 = _____ × 100 (4)

where is the conductivity in the presence of the gas being tested and is the conductivity in air ambient. In terms of the electric current measured in the semiconductor-based gas sensor on the application of a constant bias voltage:

Δ –

(%) = ___ × 100 = _____ × 100 (5)

where is the current measured in the presence of the gas being sensed and is the current measured in air (i.e., in the absence of the gas being tested).

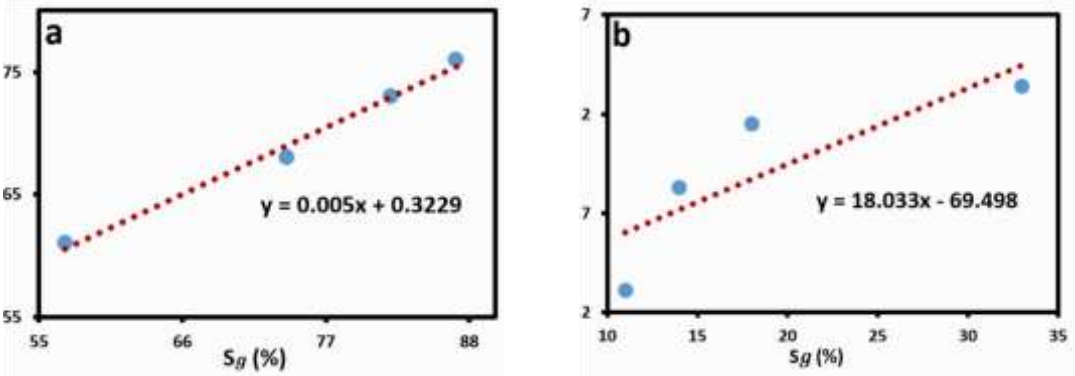

Figure 16: Relation between the sensor sensitivity and analyte concentration for NH_3 (a) and C_6H_{14} (b) gases. The blue circles are experimental data and the dark red dotted line is the linear fit result.

S of semiconducting materials gas sensors can usually be empirically represented as:

= (6)

ISSN: 1211-4401

where Pg is the tested gas partial pressure, which is direct proportion to its constant concentration(C) and exponent β is the response characteristics depending on the charge species on the surfaces and stoichiometry of the element reactions on the surfaces of nanowires [39].
As shown in Figure 16a-b, β is found to be 0.3229 (NH_3) and -69.498 (C_6H_{14}), which are similar to those of sensors reported in the literature [40].The linear dependence on $\log_{10}S_g$ to the partial pressure of gas P_g implies that the sensing mechanism follows a reversible process, which is highly desirable for sensing application.
The PPyDNA nanowire-assemblage based sensor is reversible type for NH3 and C6H14 gases detection as the response and recovery times are independent of their gaseous concentrations. These nanowires-assemblage-based gas sensors can have direct application in industrial environment because of their fast response (18 and 41 s) and recovery (28 and 45 s) times at room temperature.

Table 3: Comparison between the Present Study and the Literature of the Sensitivity, Response and
Recovery Times for the PPyDNA Nanowires -Based Gas Sensor

Nanostructure	Concentration	Temperature	Sensitivity	Response	Recovery
Nanowires (This work)	0.76 ppm	19^0C	57-87%	18-98 s	45-85 s
PPy-DBSA NCs [41]	20 ppm	25^0C	14%	205 s	134 s
PPy-ZnONCs [42]	50 ppm	RT	79%	23 s	62 s
PPy-SnO_2NCs [43]	5 ppm	RT	75%	259 s	468 s
PPy-CSA films [44]	100 ppm	RT	52%	124 s	81 s
PPy-MWCNT-ZnO [45]	200 ppm	RT	325%	2 s	-

RT= Room Temperature, NCs = Nanocomposites

Table 3 shows a comparison between the present study and similar reported PPy nanowire composite based sensors. It can be observed that PPyDNA nanowires sensor is exceedingly sensitive (87% to 0.76 ppm) to NH3 gas at room temperature as compared with previous reported results. From same table, response and recovery times shows similar pattern when compared with other similar studies.

The only exception in the comparison of the three sensing parameters was PPy-MWCNT-ZnO composite study as can be seen in the table, its higher sensitivity (325%) and quick response (2 s) at room temperature may be due to the higher electrical conductivity of the nanocomposite that can be attributed to the electrical contribution from MWCNT and ZnO that have good electrical properties.

Previous study [46] have suggested that, when small amount of ammonia comes in contact with conducting form of polypyrrole, lone pair of NH3 interact with the positive charge of polaron and bipolaron of PPy in PPyDNA, which decreases the intensity of charge and hence the mobility of charge carrier decreases resulting in the increase in resistivity. If high concentration of ammonia is exposed to conducting polymer, it is reduced to non-conducting form. Since Cl^- present in polymeric form of Polypyrrole reacts with ammonia to form $NH4Cl^-$, an increase in the resistivity of the material is observed. However the composite regains its conductivity on exposure to air.

Sensing behaviour depends upon the amount of interaction between the gas and sensing layer, the concentration of gas and degree of adsorption/desorption among others. With the increase in concentration rate of diffusion of NH_3 molecules towards polymer nanocomposite enhances, thus number of active molecules per unit volume of active sensing sites increases which leads to high gas response with lower response time. One dimensional morphology of nanocomposite provides high surface area for maximum gas adsorption leading to high sensor response. Increased rate of chemisorption at high concentration further enhances the desorption rates and sensing site renewal.

Hexane has the lowest sensitivity towards the polymers nanowires, most likely due to its low/weak adsorption of the molecules on the composite and then changes in the polymer conformation. It appears that the more polar molecules have a greater effect; presumably hexane adsorbs weakly [47].

Conclusions

A simple and practical chemiresistive type of gas sensor for NH_3 and C_6H_{14}, based on polypyrrole DNA templated nanowires has been successfully fabricated by rapid wet chemistry method. The templated nanowires have been characterized by different spectroscopic and microscopic techniques as well as current-voltage measurements that proves the nanowires to be an intimate mixture of both the PPy and DNA and at the same time having electrical conductance. The fabricated sensors have been successfully tested for NH_3 and C_6H_{14} sensing at room temperature. The experimental results disclosed that the materials are good sensors for the measured analyte at room temperature as expected of conductive polymers.

They provide several well defined advantages: fast response and recovery; easy fabrication; high repeatability, room temperature operation, enhanced sensitivity compared with other thin-film sensors at low gas concentration; high surface-to-volume ratio of nanowires that is responsible for carrier concentration on charge transfer from the surface and charge in nanowire conductance; small sample size and tunable charge transport properties as indicated in their electrical behaviour. Compared to existing metal-oxide technology the devices are simpler because they are sufficiently conductive at room temperature to not require on-chip heating. Typical commercial metal oxide vapour sensors employ localised heating on-chip to temperatures of the order of 200-400^oC to drive electron transfer reactions with the analyte and ensure the device has sufficient conductance. The research findings established that PPyDNA nanowires promise for future applications in NH_3 and C_6H_{14} gases sensing.

References

S.T. Navale, G.D. Khuspe, M.A. Chougule, V.B. Patil, J. Mater. Sci. Mater. Elec. 2014, 25, 65–75.

K. Anuar, S. Murali, A. Fariz, H.N.M. Mahmud Ekramul, Mater. Sci. 2004, 10, 255

A.B. Kaiser, Rep. Prog.Phys. 2001, 64, 1–49.

A.Kassim, Z.B. Basar, H.N.M.E. Mahmud, Chem. Sci. 2002,114, 155–162

A.A. Khan, M. Khalid and U. Baig, Reactive Funct. Pol, 2010, 70, 849–855.

A.L. Sharma, K. Kumar, A. Deep, Sens. Actuators A. 2013, 198, 107–11.

R.A. delaHoz, D.P. Schueter, W.N. Rom, Am. J. Ind. Med. 1996, 29, 209–214.

Environmental Protection Agency, Toxicological Review of n-hexane, EPA/635/R-03/012, www.epa.gov/iris (accessed on 14/09/2018)

M.T. Ramesan, V. Santhi, B.K. Bahuleyan and M.A. Al-Maghrabi, Mat. Chem. Phys. 2018, 211, 343-354.

X. Li, X. Zhang, H.Li,J. App Pol Sci,81, 2001, 3002–3007.

N. DaSilva, P.F. deOliveira, J.L. Damasceno, D.C. Tavares, A.A. Batista and G.V. Poelhsitz, Bioorg. Chem. Appl., 2017, 2017, 780-789.

A.Cheng, J. Wang, W. Chuang, Z. Liao, J. Huang, S. Huang, W. Fan and D. Lee, Polym. Chem., 2017, 8, 3294-3299.

S.M.D. Watson, H.D.A. Mohamed, B.R. Horrocks, and A. Houlton, Nanoscale, 2013.5:12, 49-59.

R. Whelan, K.R. Bambery, P. Heraud, M. J. Tobin, M. Diem, D. McNaughton and B.R. Wood, Nucleic Acids Research, 2011, 39:13, 5439–5448.

H. Huang, C. Karlsson, M. Strømme, A. Gogoll and M. Sjodin, Phys. Chem. Chem. Phys. 2017, 19, 10427-10435.

M. Choudhary, R.U.l Islam, M.J. Witcomb and K. Mallick, Dalton Trans., 2014, 43, 6396–6405.

U. Sree, Y. Yamamoto, H. Shiigi and T. Nagaoka, Synth. Met. 2002, 131, 161-165.

A. Brennan, S.J. Spencer, T. Faris, S.H. Cronin, R.P. Silva, T. Sainsbury, I.S. Gilmore, Z. Stoeva and A.J. Pollard, App. Sur. Sci., 403, 2017, 403-412.

L. Atanasoska, K. Naoi, and W.H. Smyrl, Chem. Mater., 1992, 4. 988-994.

M.G. Campbell, D. Sheberla, S.F. Liu, T.M. Swager and M. Dincă, Angew Chem Int. Ed, 2015, 54, 4349-4352.

Z. Deng, D.C. Stone, and M. Thompson, Analyst, 1996, 121, 1341-1348.

A. Briones, E. Mateo-Marti, C. Gmez-Navarro, V. Parro, E. Romn, J.A. Mart and Gago, Phys. Rev. Lett. 2004, 93, 208103-208107.

M.R. Vilar, A.M. Botelho do Rego, A.M. Ferraria, Y. Jugnet, D. Peled and R. Naaman, J. Phys. Chem. B, 2008, 112, 6957-6964.

M.M. Mahat Nanomed Nanotechnol, 2017, 2(1): 116-117.

P. Jennings, A.C. Jones, A.R. Mount, and A.D. Thomson, J. Chem. Soc. Faraday Trans., 1997, 93, 3791-3797.

J. Joo, J.K. Lee, S.Y. Lee, K.S. Jang, E.J. Oh and A. J. Epstein, Macromolecules, 2000, 33, 51315136.

W. E. Harnack, A. Ford, Yasuda and J.M. Wessels, Nano Lett. 2000, 2, 919-933.

M.L. Malone and B.M. Paegel, ACS Comb. Sci. 2016, 18, 182–187.

S. Pruneanu, S.A. Al-Said, L. Dong, T.A. Hollis, M.A. Galindo, N.G. Wright, A. Houlton, and B.R. Horrocks, Adv.Funct.Mater.2008, 18, 2444-2454.

S.M. Watson, A.R. Pike, J. Pate, A. Houlton, B.R. Horrocks, Nanoscale, 2014, 6, 27-37.

X.S. Du, M. Xiao and Y.Z. Meng. 2004.J. Pol. Sci. 42, 1972–1978.

N. Su, H.B. Li, S. Yuan, P. Yi and E.Q. Yin, eXPRESS Polymer Lets, 2012, 6, 697-705 33. P. Mazumdar, S. Chockalingam, S. Rattan and B.K. Gupta, ACS Omega, 2018, 3, 3675–3687.

Z.X. Deng and C.D. Mao, Nano Lett., 2003, 3, 1545-1548.

L. Dong, T. Hollis, B.A. Connolly, N.G. Wright, B.R. Horrocks and A. Houlton, Adv. Mater., 2007, 19, 1748-1751.

A.A. Khan, R. Ahmad and M. Zeeshan, Anal Chem Res, 2017, 12, 52-64.

R. Hassanien, S.A. Farha, S. Lidija, L. Ross and N.G. Wright, Nanotechnology, 2012, 23(7), 601-612.

G. Korotcenkov, Mater. Sci. Eng., B 2007, 139, 1–23.

Q. Wan, Q.H. Li, Y.J. Chen, T.H. Wang, X.L. He, J.P. Li and C.L. Lin, Appl. Phys. Lett. 2004, 84, 3654–3656.

J. Guo, J. Zhang, M. Zhu, D. Ju, H. Xu and B. Cao, Sens. Actuators, B 2014, 199, 339-345.

F. Merdj, A. Mekki, D. Guettiche, B. Mettai, Z.B.D. Sayah, Z. Safidine, A. Abdi, R. Mahmoud and

M.M. Chehimi, Macromol. Res., 2018, 26(6), 511-520.

S. Jain, N. Karmaka, A. Shah, D.C. Kothari, S. Mishra and N.G. Shimpi, App. Sur. Sci., 2017, 396, 1317–1325.

Y. Li, H. Ban and M. Yang, Sens Actuators B, 2016, 224, 449-457.

S.T. Navale, M.A. Chougule, V.B. Patil and A.T. Mane, Synthetic Metals, 2014, 189, 111–118.

C. Mahajan, P. Chaudhari and S. Mishra, J. Mat. Sci.: Mat. Elec. 2018. 29, 8039-8048.

O. Ansari, S.P. Ansari, S.K. Yadav, T. Anwer, M.H. Cho, F. Mohammad, J. Ind. Eng. Chem., 2014, 20, 2010-2017

S.J. Park, C. S. Park and H. Yoon, Polymers, 2017, 9, 155.

ISSN: 1211-4401